VOL. 11, NO. 15, AUGUST 2016 ISSN 1819-6608
ARPN Journal of Engineering and Applied Sciences

www.arpnjournals.com

EFFECTS OF ASSEMBLY ERRORS ON TOOTH CONTACT ELLIPSES AND TRANSMISSION ERRORS OF A DOUBLE-CROWNED MESHING GEAR PAIR

Van-The Tran
Department of Mechanical Engineering, Hung Yen University of Technology and Education, 5 Rd., Hung Yen City, Vietnam
E-Mail: vanct4.hut@gmail.com

ABSTRACT

A helical gear is crowned in both the cross-profile and longitudinal directions called a double-crowned gear. The tooth surface of the gear can be generated by hobbing, shaving, honing processes. In this paper, the hobbing process is used for double-crowning the tooth surface of work gear with three different hobbing methods included conventional method, variable tooth thickness (VTT) method and modifying the work gear rotation angle method. A computer simulation example is implemented to compare the meshing-conditions, contact ellipses, and transmission errors under various assembly errors of the double-crowned gear pairs that are generated by the three hobbing methods.

Keywords: double crowned gear, modified rotation angle, tooth contact analysis, contact ellipse, transmission error.

INTRODUCTION

The double-crowned helical gear surfaces are particularly important for misaligned assembly gear pairs that improve bearing contact and reduce noise. One of the most productive and economical methods for manufacturing such gears is hobbing. By conventional method, two crowning processes are used to generate double-crowned tooth flanks on a helical gear. One crowning process is accomplished in the cross-profile direction by modifying the hob cutter profile to a parabolic curve and the other is achieved in the longitudinal direction by varying the center distance between the hob and work gear. However, it induces twisted flanks on the generated work gear's tooth surfaces. By variable tooth thickness (VTT) hobbing method, the standard hob cutter must be reground and it increases production costs. In this paper, a hobbing method for double-crowning the tooth flank of helical gears by modifying the work gear rotation angle without modifying the hob cutter tooth profile or varying the center distance during the gear hobbing process is applied.

The overall geometry, design, and manufacture of a conventional involute helical gear are detailed in textbooks by Litvin and Fuentes [1]. In 2001, Litvin *et al*. [2] patented a design for helical and spur gear drives with double-crowned pinion tooth surfaces that generate a predesigned parabolic transmission error function in the meshing process to reduce vibration and noise of a mating gear set. Litvin et al. [3] also proposed a method for modifying the conventional involute helical gear by conjugating a double-crowned gear with a conventional helical involute gear. Litvin et al. [4] outlined a new topology of modified helical gear tooth surfaces based on profile and longitudinal crowning. This latter is used involute and crowned zones to localize the bearing contact in the presence of misalignments. Subsequently, Wang and Fong [5] proposed a novel face-hobbing method to generate spur gears using lengthwise crowning by two head cutters that formed imaginary generating rack with cycloidal lengthwise tooth traces. Winkel [6] then proposed a special profile modification in hob finishing that produces topological tooth flank modifications with free of twist. More recently, Hsu and Fong [7] patented the design of a longitudinally variable tooth thickness (VTT) hob and a hobbing method with diagonal feed that needs no variation of center distance. Of particular relevance to our verification techniques, Tsay [8], in a much earlier paper, developed a tooth contact analysis computer program for simulating gear meshing and bearing contact, and investigated the influence of gear misalignment on kinematic errors. Lastly, Hsu and Su [9] investigated the gear tooth surface topologies, contact ellipses, and transmission errors of work gear pairs generated by a modified hob with variable tooth thickness. Tran et al. [10, 11] proposed two novel hobbing methods to generate anti-twist tooth flanks of the helical gear in longitudinal tooth crowning. And Tran *et al.* [12] analysed the contact ellipses and transmission errors for a crowned gear pair that is generated by a dual-lead hob cutter.

This paper studies the effects of assembly error conditions on the tooth contact ellipses, contact points, and transmission errors in the meshing of the work gear pair. These errors have much effects on the dislocation of the center contact point particularly the vertical misaligned angle and the horizontal misaligned angle. Transmission errors of the gear pairs are in fact a parabolic function, and the maximum magnitude of transmission errors are negligible.

COMPUTER SIMULATION OF MESHING AND TOOTH CONTACT ANALYSIS

Tooth contact analysis is usually used to verify the contact pattern and kinematic characteristics of meshing gear pairs that includes the contact point path and contact ellipses. We simulate the conditions of meshing and contact [1] by applying the tooth contact analysis (TCA) to the meshing gear pair composed of a standard involute helical gear 3 and the proposed double-crowned involute helical pinion 2, whose tooth surface mating equations are represented in the same coordinated system.

The coordinate systems for gear meshing are shown in Figure-1, wherein coordinate systems $S_2(x_2, y_2, z_2)$ and $S_3(x_3, y_3, z_3)$ are rigidly connected to the double-crowned helical pinion 2 and standard involute helical gear 3, respectively. The auxiliary coordinate systems $S_h(x_h, y_h, z_h)$, $S_i(x_i, y_i, z_i)$, and $S_j(x_j, y_j, z_j)$ are used for simulating gear set assembly errors between the double-crowned helical pinion 2 and standard involute helical gear 3, including center distance error ΔE, horizontal misaligned angle $\Delta\gamma_h$ in the axial direction, and vertical misaligned angle $\Delta\gamma_v$ in the radial direction.

By applying the homogeneous coordinate transformations method, transforming from the coordinate system $S_2(x_2, y_2, z_2)$ to fixed coordinate system $S_h(x_h, y_h, z_h)$, the tooth surface equations and surface unit normal of the pinion 2 can be represented in the fixed coordinate system S_h as follows:

$$\mathbf{r}_h^{(2)}(u_1, v_1, \psi_1, \phi_1, z_a(t), \phi_2) = \mathbf{M}_{h2}\mathbf{r}_2^{(2)}(u_1, v_1, \psi_1, \phi_1, z_a(t)), \quad (1)$$

$$\mathbf{n}_h^{(2)}(u_1, v_1, \psi_1, \phi_1, z_a(t), \phi_2) = \mathbf{L}_{h2}\mathbf{n}_2^{(2)}(u_1, v_1, \psi_1, \phi_1, z_a(t)), \quad (2)$$

where $\mathbf{M}_{h2} = \mathbf{M}_{hi}\mathbf{M}_{ij}\mathbf{M}_{j2}$, (3)

$$\mathbf{M}_{j2} = \begin{bmatrix} \cos\phi_2 & \sin\phi_2 & 0 & 0 \\ -\sin\phi_2 & \cos\phi_2 & 0 & 0 \\ 0 & 0 & 1 & 0 \\ 0 & 0 & 0 & 1 \end{bmatrix}, \quad (4)$$

$$\mathbf{M}_{ij} = \begin{bmatrix} \cos\Delta v & 0 & \sin\Delta v & 0 \\ 0 & 1 & 0 & 0 \\ -\sin\Delta v & 0 & \cos\Delta v & 0 \\ 0 & 0 & 0 & 1 \end{bmatrix}, \quad (5)$$

and $$\mathbf{M}_{hi} = \begin{bmatrix} 1 & 0 & 0 & 0 \\ 0 & \cos\Delta h & \sin\Delta h & 0 \\ 0 & -\sin\Delta h & \cos\Delta h & 0 \\ 0 & 0 & 0 & 1 \end{bmatrix}. \quad (6)$$

vector's transformation matrix $\mathbf{L}_{h2}$ is the sub-matrix of $\mathbf{M}_{h2}$ by deleting the last column and row.

After some mathematical operations, the locus and unit normal vector of involute helical pinion 2 can be simplified as:

$$\mathbf{r}_h^{(2)}(u_1, v_1, \psi_1, \phi_1, z_a(t), \phi_2) = \begin{bmatrix} x_h^{(2)}(u_1, v_1, \psi_1, \phi_1, z_a(t), \phi_2) \\ y_h^{(2)}(u_1, v_1, \psi_1, \phi_1, z_a(t), \phi_2) \\ z_h^{(2)}(u_1, v_1, \psi_1, \phi_1, z_a(t), \phi_2) \\ 1 \end{bmatrix}, \quad (7)$$

$$\mathbf{n}_h^{(2)}(u_1, v_1, \psi_1, \phi_1, z_a(t), \phi_2) = \begin{bmatrix} n_{x_h^{(2)}}(u_1, v_1, \psi_1, \phi_1, z_a(t), \phi_2) \\ n_{y_h^{(2)}}(u_1, v_1, \psi_1, \phi_1, z_a(t), \phi_2) \\ n_{z_h^{(2)}}(u_1, v_1, \psi_1, \phi_1, z_a(t), \phi_2) \end{bmatrix}, \quad (8)$$

where

$$x_h^{(2)} = \cos\Delta v(x_2\cos\phi_2 + y_2\sin\phi_2) + \sin\Delta v[z_2\cos\Delta h + \sin\Delta h(-y_2\cos\phi_2 + x_2\sin\phi_2)], \quad (9)$$

$$y_h^{(2)} = z_2\sin\Delta h + \cos\Delta h(y_2\cos\phi_2 - x_2\sin\phi_2), \quad (10)$$

$$z_h^{(2)} = z_2\cos\Delta v\cos\Delta h - \sin\Delta v(y_2\sin\phi_2 + x_2\cos\phi_2) + \cos\Delta v\sin\Delta h(x_2\sin\phi_2 - y_2\cos\phi_2), \quad (11)$$

$$n_{x_h^{(2)}} = \cos\Delta v(n_{x_2}\cos\phi_2 + n_{y_2}\sin\phi_2) + \sin\Delta v[n_{z_2}\cos\Delta h + \sin\Delta h(-n_{y_2}\cos\phi_2 + n_{x_2}\sin\phi_2)], \quad (12)$$

$$n_{y_h^{(2)}} = n_{z_2}\sin\Delta h + \cos\Delta h(n_{y_2}\cos\phi_2 - n_{x_2}\sin\phi_2), \quad (13)$$

$$n_{z_h^{(2)}} = n_{z_2}\cos\Delta v\cos\Delta h - \sin\Delta v(n_{y_2}\sin\phi_2 + n_{x_2}\cos\phi_2) + \cos\Delta v\sin\Delta h(n_{x_2}\sin\phi_2 - n_{y_2}\cos\phi_2). \quad (14)$$

Similarly, the tooth surface equations and surface unit normal of the gear 3 can be represented in the fixed coordinate system $S_h(x_h, y_h, z_h)$ as follows:

$$\mathbf{r}_h^{(3)}(u_3, v_3, \psi_3, \phi_3) = \mathbf{M}_{h3}\mathbf{r}_3^{(3)}(u_3, v_3, \psi_3), \quad (15)$$

$$\mathbf{n}_h^{(3)}(u_3, v_3, \psi_3, \phi_3) = \mathbf{L}_{h3}\mathbf{n}_3^{(3)}(u_3, v_3, \psi_3), \quad (16)$$

where $\mathbf{M}_{h3} = \mathbf{M}_{hg}\mathbf{M}_{g3}$, (17)

$$\mathbf{M}_{g3} = \begin{bmatrix} \cos\phi_3 & -\sin\phi_3 & 0 & 0 \\ \sin\phi_3 & \cos\phi_3 & 0 & 0 \\ 0 & 0 & 1 & 0 \\ 0 & 0 & 0 & 1 \end{bmatrix}, \quad (18)$$

and $\mathbf{M}_{hg} = \begin{bmatrix} \cos\pi & \sin\pi & 0 & E_o + \Delta E \\ -\sin\pi & \cos\pi & 0 & 0 \\ 0 & 0 & 1 & 0 \\ 0 & 0 & 0 & 1 \end{bmatrix}$. (19)

Vector's transformation matrix $\mathbf{L}_{h3}$ is the sub-matrix of $\mathbf{M}_{h3}$ by deleting the last column and row.

After some mathematical operations, the locus and unit normal vector of standard involute helical gear 3 can be simplified as:

$$\mathbf{r}_h^{(3)}(u_3, v_3, \phi_3) = \begin{bmatrix} x_h^{(3)}(u_3, v_3, \psi_3, \phi_3) \\ y_h^{(3)}(u_3, v_3, \psi_3, \phi_3) \\ z_h^{(3)}(u_3, v_3, \psi_3, \phi_3) \\ 1 \end{bmatrix}, \quad (20)$$

$$\mathbf{n}_h^{(3)}(u_3, v_3, \phi_3) = \begin{bmatrix} n_{x_h^{(3)}}(u_3, v_3, \psi_3, \phi_3) \\ n_{y_h^{(3)}}(u_3, v_3, \psi_3, \phi_3) \\ n_{z_h^{(3)}}(u_3, v_3, \psi_3, \phi_3) \end{bmatrix}, \quad (21)$$

where

$$x_h^{(3)} = E_o + \Delta E - x_3 \cos\phi_3 + y_3 \sin\phi_3, \quad (22)$$

$$y_h^{(3)} = -x_3 \sin\phi_3 - y_3 \cos\phi_3, \quad (23)$$

$$z_h^{(3)} = z_3, \quad (24)$$

$$n_{x_h^{(3)}} = -n_{x_3} \cos\phi_3 + n_{y_3} \sin\phi_3, \quad (25)$$

$$n_{y_h^{(3)}} = -n_{y_3} \cos\phi_3 - n_{x_3} \sin\phi_3, \quad (26)$$

and $n_{z_h^{(3)}} = n_{z_3}$. (27)

According to the conditions of meshing and contact of an involute helical gear pair, the mating surfaces must satisfy the condition of tooth continuous tangency at the point of contact. Thus the tooth surfaces of the pinion 2 and gear 3 must have a common contact point that can be determined at their contact point by the position vectors $\mathbf{r}_h^{(2)}$ and $\mathbf{r}_h^{(3)}$, as shown in Eq. (28), and a common unit normal vector $\mathbf{n}_h^{(2)}$ and $\mathbf{n}_h^{(3)}$, as shown in Eq. (29). These relations are expressed as follows:

$$\mathbf{r}_h^{(2)}(u_1, v_1, \psi_1, \phi_1, z_a(t), \phi_2) = \mathbf{r}_h^{(3)}(u_3, v_3, \psi_3, \phi_3), \quad (28)$$

$$\mathbf{n}_h^{(2)}(u_1, v_1, \psi_1, \phi_1, z_a(t), \phi_2) = \mathbf{n}_h^{(3)}(u_3, v_3, \psi_3, \phi_3). \quad (29)$$

In three-dimensional space, Eq. (28) contains three independent equations and Eq. (29) contains two independent equations because it is constrained by the relation of the unit normal vector $\left|\mathbf{n}_h^{(2)}\right| = \left|\mathbf{n}_h^{(3)}\right| = 1$. So we have the five independent equations together with the two equations for meshing between the surfaces of the rack cutter and blank pinion, and rack cutter and blank gear and two equations for meshing between the surfaces of the hob cutter and work [16]. Therefore, a system of nine independent equations with ten unknowns, u_1, v_1, ψ_1, ϕ_1, $z_a(t)$, ϕ_2, u_3, v_3, ψ_3 and ϕ_3, can be established. The variable ϕ_2 can be considered an input variable, leaving other nine variables to be solved by nine independent equations with nine unknowns.

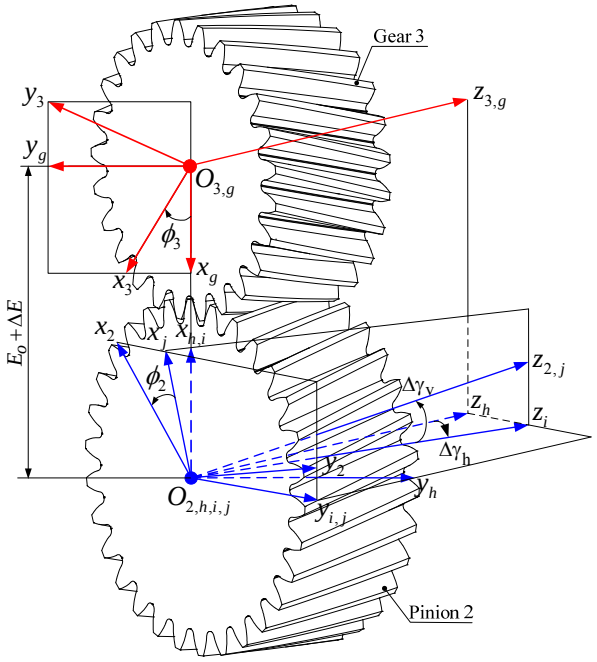

Figure-1. Simulation of meshing gear pairs with gear assembly errors.

CONTACT ELLIPSE ANALYSIS

Under applied load, the instantaneous contact of pinion 2 and gear 3 surfaces at a point is spread over an elliptical area due to elasticity of tooth surfaces. The symmetry center of the instantaneous contact ellipse coincides with the theoretical tangency point. The bearing contact is formed as a set of contact ellipses. The orientation and dimensions of the contact ellipses on standard involute gear 3 surface are determined by considering the elastic deformation of the pinion 2 and gear 3 surfaces at the theoretical point of tangency M (δ), as shown in Figure-2. The elastic deformation is expressed as follows:

$$\delta = \delta_1 + \delta_2, \quad (30)$$

where δ_1 and δ_2 are deformations of contacting pinion 2 and gear 3 surfaces at common contact point M, respectively. The elastic deformation depends on the applied load and considers as a given value $(\delta = 0.006mm)$.

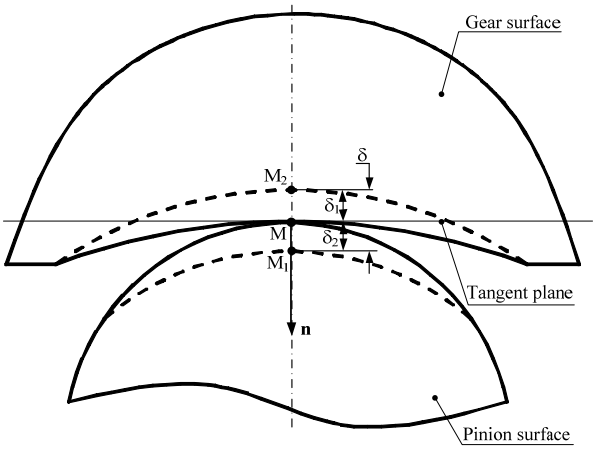

Figure-2. Elastic deformations of the pinion 2 and gear 3.

In addition, the contact ellipse also depends on the principal curvatures of the contacting surfaces, angle σ_1 is formed between the unit vectors of the principal directions $\mathbf{e}_1^{(2)}$ and $\mathbf{e}_1^{(3)}$ that represent the principal directions on the surfaces of pinion 2 and gear 3, as shown in Figure-3.

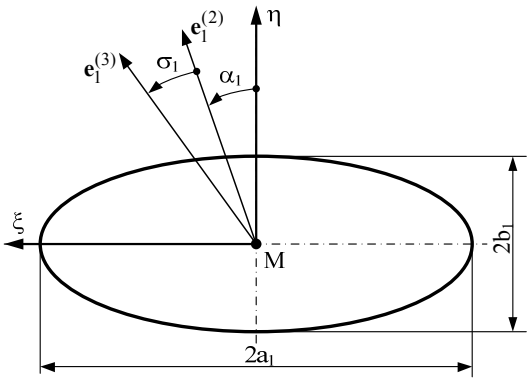

Figure-3. Parameters of contact ellipse on the gear 3.

The locus $\mathbf{r}_3$ and unit normal vector $\mathbf{n}_3$ of the standard involute gear 3 are expressed in Eqs. (20) and (21), respectively. The principal curvatures $k_f^{(3)}$ and $k_h^{(3)}$ of the standard involute gear 3 at the contact point M, and the unit vectors $\mathbf{e}_f^{(3)}$ and $\mathbf{e}_h^{(3)}$ of surface can be determined from the following system of equations

$$k_f^{(3)} = 0, \tag{31}$$

$$k_h^{(3)} = \frac{\left(\mathbf{r}_{3,\psi_3\psi_3}.\mathbf{n}_3\right)\left(\mathbf{r}_{3,v_3}.\mathbf{r}_{3,v_3}\right)}{\left(\mathbf{r}_{3,\psi_3}.\mathbf{r}_{3,\psi_3}\right)\left(\mathbf{r}_{3,v_3}.\mathbf{r}_{3,v_3}\right)-\left(\mathbf{r}_{3,v_3}.\mathbf{r}_{3,\psi_3}\right)^2}, \tag{32}$$

$$\mathbf{e}_f^{(3)} = \frac{\mathbf{r}_{3,v_3}}{\sqrt{\mathbf{r}_{3,v_3}.\mathbf{r}_{3,v_3}}}, \tag{33}$$

$$\text{and } \mathbf{e}_h^{(3)} = \frac{\mathbf{r}_{3,v_3}-\left(\frac{\mathbf{r}_{3,v_3}.\mathbf{r}_{3,v_3}}{\mathbf{r}_{3,v_3}.\mathbf{r}_{3,\psi_3}}\right)\mathbf{r}_{3,\psi_3}}{\sqrt{\left(\mathbf{r}_{3,v_3}-\left(\frac{\mathbf{r}_{3,v_3}.\mathbf{r}_{3,v_3}}{\mathbf{r}_{3,v_3}.\mathbf{r}_{3,\psi_3}}\right)\mathbf{r}_{3,\psi_3}\right).\left(\mathbf{r}_{3,v_3}-\left(\frac{\mathbf{r}_{3,v_3}.\mathbf{r}_{3,v_3}}{\mathbf{r}_{3,v_3}.\mathbf{r}_{3,\psi_3}}\right)\mathbf{r}_{3,\psi_3}\right)}}, \tag{34}$$

where $\mathbf{r}_{3,\psi_3} = \frac{\partial \mathbf{r}_3}{\partial \psi_3}$, $\mathbf{r}_{3,\psi_3\psi_3} = \frac{\partial^2 \mathbf{r}_3}{\partial \psi_3^2}$, and $\mathbf{r}_{3,v_3} = \frac{\partial \mathbf{r}_3}{\partial v_3}$.

The locus $\mathbf{r}_2$ and unit normal $\mathbf{n}_2$ of the pinion 2 are expressed in Eqs. (7) and (8), respectively. The principal curvatures $k_f^{(2)}$ and $k_h^{(2)}$ of the pinion 2 at the contact point M can be determined from the following system of equations:

$$k_f^{(2)} = \frac{(\mathbf{r}_{2,u_1u_1}.\mathbf{n}_2)h_5 + \mathbf{r}_{2,u_1v_1}.\mathbf{n}_2}{(\mathbf{r}_{2,u_1}.\mathbf{r}_{2,u_1})h_5 + \mathbf{r}_{2,u_1}.\mathbf{r}_{2,v_1}}, \tag{35}$$

$$k_h^{(2)} = \frac{(\mathbf{r}_{2,u_1u_1}.\mathbf{n}_2).h_4 + \mathbf{r}_{2,u_1v_1}.\mathbf{n}_2}{(\mathbf{r}_{2,u_1}.\mathbf{r}_{2,u_1})h_4 + \mathbf{r}_{2,u_1}.\mathbf{r}_{2,v_1}}, \tag{36}$$

$$\mathbf{e}_f^{(2)} = \frac{\mathbf{r}_{2,u_1}.h_5 + \mathbf{r}_{2,v_1}}{\sqrt{(\mathbf{r}_{2,u_1}.h_5 + \mathbf{r}_{2,v_1}).(\mathbf{r}_{2,u_1}.h_5 + \mathbf{r}_{2,v_1})}}, \tag{37}$$

$$\text{and } \mathbf{e}_h^{(2)} = \frac{\mathbf{r}_{2,u_1}.h_4 + \mathbf{r}_{2,v_1}}{\sqrt{(\mathbf{r}_{2,u_1}.h_4 + \mathbf{r}_{2,v_1}).(\mathbf{r}_{2,u_1}.h_4 + \mathbf{r}_{2,v_1})}}. \tag{38}$$

with

$$h_1 = (\mathbf{r}_{2,u_iu_i}.\mathbf{n}_2)(\mathbf{r}_{2,u_1}.\mathbf{r}_{2,v_1}) - (\mathbf{r}_{2,u_1v_1}.\mathbf{n}_2)(\mathbf{r}_{2,u_1}.\mathbf{r}_{2,u_1}), \tag{39}$$

$$h_2 = (\mathbf{r}_{2,u_1u_1}.\mathbf{n}_2)(\mathbf{r}_{2,v_1}.\mathbf{r}_{2,v_1}) - (\mathbf{r}_{2,v_1v_1}.\mathbf{n}_2)(\mathbf{r}_{2,u_1}.\mathbf{r}_{2,u_1}), \tag{40}$$

$$h_3 = (\mathbf{r}_{2,u_1v_1}.\mathbf{n}_2)(\mathbf{r}_{2,v_1}.\mathbf{r}_{2,v_1}) - (\mathbf{r}_{2,v_1v_1}.\mathbf{n}_2)(\mathbf{r}_{2,u_1}.\mathbf{r}_{2,v_1}), \tag{41}$$

$$h_4 = \frac{-h_2 - \sqrt{h_2^2 - 4h_1h_3}}{2h_1}, \tag{42}$$

$$\text{and } h_5 = \frac{-h_2 + \sqrt{h_2^2 - 4h_1h_3}}{2h_1}. \tag{43}$$

where $\mathbf{r}_{2,u_1} = \frac{\partial \mathbf{r}_2}{\partial u_1}$, $\mathbf{r}_{2,u_1u_1} = \frac{\partial^2 \mathbf{r}_2}{\partial u_1^2}$, $\mathbf{r}_{2,v_1} = \frac{\partial \mathbf{r}_2}{\partial v_1}$, $\mathbf{r}_{2,v_1v_1} = \frac{\partial^2 \mathbf{r}_2}{\partial v_1^2}$ and $\mathbf{r}_{2,u_1v_1} = \frac{\partial^2 \mathbf{r}_2}{\partial u_1 \partial v_1}$.

The angle σ_1, formed by two principal directions $\mathbf{e}_1^{(2)}$ and $\mathbf{e}_1^{(3)}$, is determined by using the equation as follows:

$$\sigma_1 = \arctan\left(\frac{\mathbf{e}_2^{(2)}.\mathbf{e}_1^{(3)}}{\mathbf{e}_1^{(2)}.\mathbf{e}_1^{(3)}}\right), \quad (44)$$

where the principal directions $\mathbf{e}_1^{(2)}$, $\mathbf{e}_2^{(2)}$ and $\mathbf{e}_1^{(3)}$ are $\mathbf{e}_1^{(3)} = \mathbf{e}_f^{(2)}$, $\mathbf{e}_1^{(2)} = \mathbf{e}_f^{(3)}\mathbf{L}_{i3}$, and $\mathbf{e}_2^{(2)} = \mathbf{e}_h^{(3)}\mathbf{L}_{i3}$, $\mathbf{L}_{i3}$ is vector's transformation matrix.

The orientation of the contact ellipse is determined with angle α_1, as shown in Figure-3, and this angle can be represented by the following equation:

$$\alpha_1 = \frac{1}{2}\arctan\left(\frac{g_3 \sin 2\sigma_1}{g_2 - g_3 \cos 2\sigma_1}\right), \quad (45)$$

where

$$g_i = k_f^{(i)} - k_h^{(i)}. \quad (i = 2,3) \quad (46)$$

The axes of the contact ellipse are determined as follows:

$$2a_1 = 2\sqrt{\left|\frac{\delta}{A_1}\right|}, \quad (47)$$

and

$$2b_1 = 2\sqrt{\left|\frac{\delta}{B_1}\right|}, \quad (48)$$

where

$$A_1 = \frac{1}{4}\left[k_2 - k_3 - \sqrt{g_2^2 - 2g_2g_3\cos 2\sigma_1 + g_3^2}\right], \quad (49)$$

$$B_1 = \frac{1}{4}\left[k_2 - k_3 + \sqrt{g_2^2 - 2g_2g_3\cos 2\sigma_1 + g_3^2}\right], \quad (50)$$

and $k_i = k_f^{(i)} + k_h^{(i)}$. $(i = 2,3)$ (51)

TRANSMISSION ERRORS

The gear's rotational angle ϕ_3 is a function of the pinion's rotational angle ϕ_2 and this function can be denoted as $\phi_3(\phi_2)$. Under the ideal meshing condition (i.e., without assembly errors), the gear's rotational angle is a linear function and equals the product of pinion's rotational angle and the pinion-gear ratio that can be expressed by

$$\phi_3(\phi_2) = \frac{N_2}{N_3}\phi_2, \quad (52)$$

where N_2 and N_3 denote the teeth numbers of the pinion 2 and gear 3, respectively.

Under a real meshing condition with assembly errors and manufacturing errors, the function $\phi_3(\phi_2)$ is a linear discontinuous function and its deviation from the linear function is defined as the transmission errors of the mating gear pair $\Delta\phi_3(\phi_2)$ that can be expressed as follows:

$$\Delta\phi_3(\phi_2) = \phi_3(\phi_2) - \frac{N_2}{N_3}\phi_2. \quad (53)$$

This linear discontinuous function can be absorbed by a predesigned parabolic function of transmission errors. This is the key for reduction of noise and vibration of gear drives. The parabolic function of transmission errors can be obtained by tooth crowning in cross-profile direction of the pinion 2. The predesigned parabolic function of transmission error $\Delta\phi_3(\phi_2)$, inducing by assembly errors of an involute helical gear set, is determined by:

$$\Delta\phi_3(\phi_2) = -a_{pr}\phi_2^2, \quad (54)$$

The double crowning method also allows us to obtain a predesigned parabolic function of transmission error $\Delta\phi_3(\phi_2)$ induced by assembly errors of the involute helical gear set:

$$\Delta\phi_3(\phi_2) = \phi_3(\phi_2) - \frac{N_2}{N_3}\phi_2 = -a_{pr}\phi_2^2 \quad (55)$$

where a_{pr} is a parabolic coefficient of the transmission error function, and $\phi_3(\phi_2)$ is the gear's rotation angle represented as a function of the pinion's rotation angle (ϕ_2).

NURMERICAL EXAMPLE

The effects of assembly error conditions on the tooth contact ellipses, contact points on gear 3, and

transmission errors in the meshing of the work gear pair are investigated. The basic parameters for the double-crowned helical pinion 2 and standard helical gear 3 and the basic coefficients for Cases A, B and C are given in Tables 1 and 2. Our analysis focuses on three specific aspects: the gear meshing center distance error, the vertical misaligned angle, and the horizontal misaligned angle.

Table-1. Basic parameters for the double-crowned helical pinion 2 and standard helical gear 3.

Gear pair data	Gear 2	Gear 3
Number of teeth (N_2)	60	60
Normal module (m_{pn})	2.5	2.5
Normal circular tooth thickness (s_{pn2})	4.712 mm	4.712 mm
Normal pressure angle (α_{pn})	20°	20°
Face width	14 mm	14 mm
Helix angle (β_{p2})	25° R.H.	25° L.H.
Outer diameter	170.506mm	170.506mm
Form diameter	160.648mm	160.648mm
Operating center distance for gear pairs meshing	165.507mm	

Table-2. Basic coefficient data.

	a (mm^{-1})	b (mm^{-1})	c	d
Case A	0.70×10^{-3}	0	-2.519	0.002
Case B	0	8.10×10^{-8}	-2.519	0.002
Case C	0	0	0	0

Gear meshing center distance error

The shifts of bearing contacts and transmission errors caused by the gear meshing center distance error ($\Delta E = 0.5mm(\Delta E / E = 0.3\%)$) in Cases A, B and C are shown in Figures 4 and 5. In this case, the contact ellipses are drawn correspondingly to the rotation angle of pinion 2 from -3.6^o to 2.4^o in Cases A and Case B and from -3.2^o to 2.8^o in Case C, as shown in Figure-4. The distributions of contact points in the longitudinal direction and dislocations of the center contact points for the three cases have small changes. It shows that the double-crowned work gears for the three cases are not sensitive to the center distance error. Figure-5 reveals that the maximum magnitude of transmission error in Case C $(\Delta\phi_{3'} = 4.9arc\sec)$ is much lower than those in Cases A $(\Delta\phi_{3'} = 8.4arc\sec)$ and B $(\Delta\phi_{3'} = 11.7arc\sec)$.

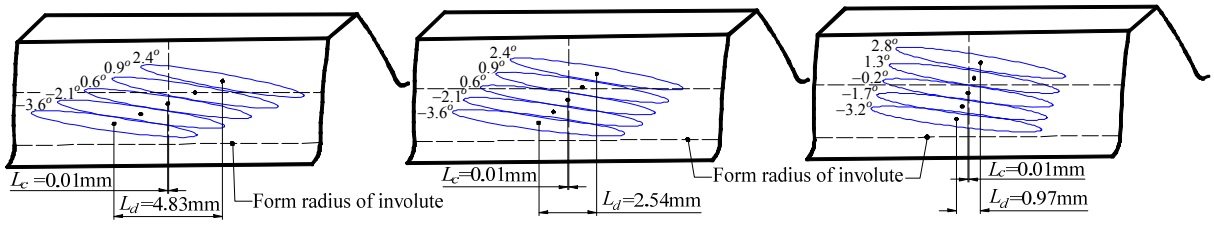

(a)Case A (b)Case B (c)Case C

Figure-4. Simulated tooth contact ellipses and contact points of the gear pairs under center distance error $\Delta E = 0.5mm$.

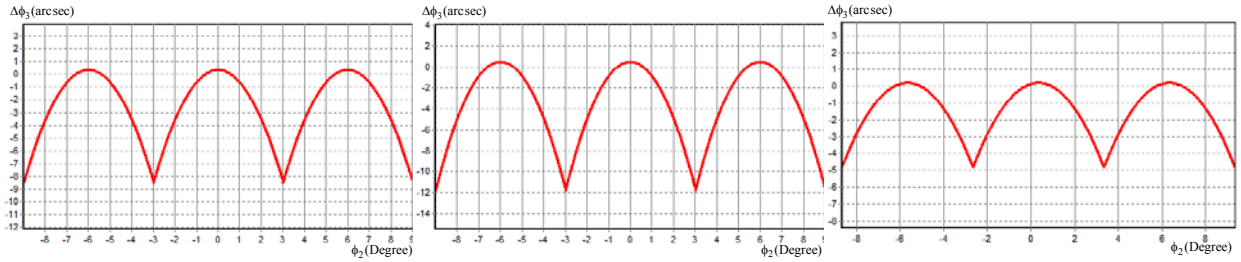

(a)Case A (b)Case B (c)Case C

Figure-5. Transmission errors of the gear pairs under center distance error $\Delta E = 0.5mm$.

Vertical misaligned angle

The influences of a vertical misaligned angle ($\Delta\gamma_v = 0.1^\circ$) on Cases A, B and C are illustrated by Figures 6 and 7. The contact ellipses are drawn correspondingly to the rotation angle of pinion 2, Cases A ($\phi_{2'} = -2.7^o,...,3.3^o$), Case B ($\phi_{2'} = -3.1^o,...,2.9^o$) and Case C ($\phi_{2'} = -3.3^o,...,2.7^o$), as shown in Figure-6. According to Figure-6, the distributions of contact points in the longitudinal direction for the three cases have small changes, but the dislocations of the center contact points in Cases A and B increase from $L_c = 0.01mm$ (Figure-4) under the center distance error to $L_c = 0.99mm$ (Figure-6(a)) and $L_c = 0.79mm$ (Figure-6(b)) with the vertical misaligned angle. Such center contact point dislocation in Case A is particularly affected by the vertical misaligned angle inducing edge contact in gear 3. The double-crowned work gear in Case C is also quite sensitive to the vertical misaligned angle, as show in Figure-6(c). However, the distributions of contact points and contact ellipses in this case are quite small, and can avoid the inducement of edge contact on gear 3. Once again, as shown in Figure-7, the maximum magnitude of transmission error in Case C ($\Delta\phi_{3'} = 4.8arc\sec$) is smaller than those in Case A ($\Delta\phi_{3'} = 8.3arc\sec$) and Case B ($\Delta\phi_{3'} = 11.8arc\sec$).

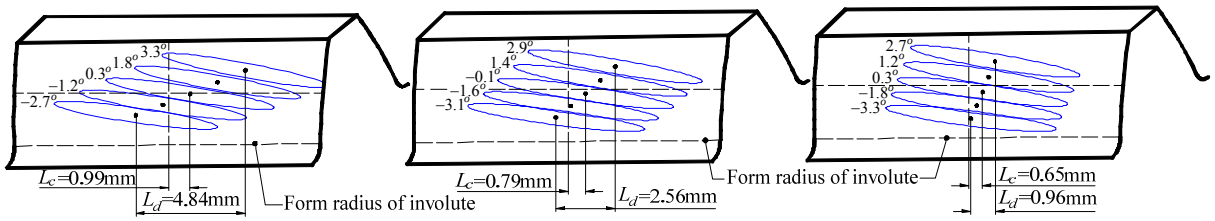

(a)Case A (b)Case B (c)Case C

Figure-6. Simulated tooth contact ellipses and contact points with vertical misalignment $\Delta\gamma_v = 0.1^\circ$.

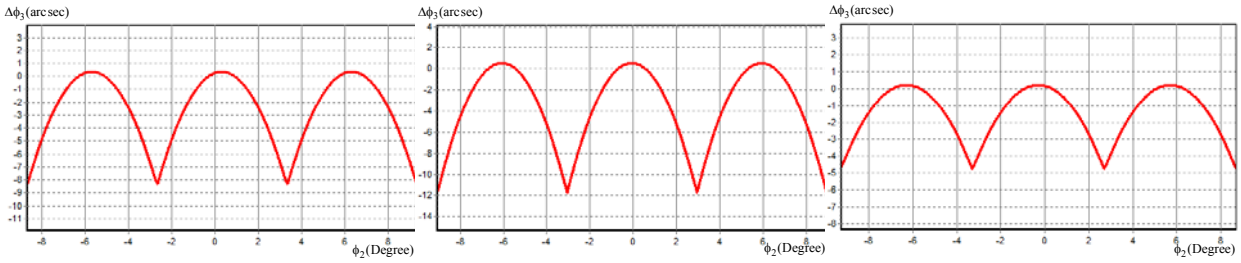

(a)Case A (b)Case B (c)Case C

Figure-7. Transmission errors of the gear pairs with vertical misalignment $\Delta\gamma_v = 0.1^\circ$.

Horizontal misaligned angle

The horizontal misaligned angle ($\Delta\gamma_h = 0.1^\circ$) has the greatest effect on the dislocation of the center contact point in three cases, as shown in Figure-8. Wherein, the contact ellipses are drawn correspondingly to the rotation angle of pinion 2, Cases A ($\phi_{2'} = -2.1^o,...,3.9^o$), Case B ($\phi_{2'} = -3.1^o,...,2.9^o$) and Case C ($\phi_{2'} = -4.2^o,...,1.8^o$). Specifically, the dislocations of the center contact points in Cases A and B increase greatly from zero (Figure-4(a) and Figure-4(b)) to 2.83 mm (Figure-8(a)) and 2.32 mm

(Figure-8(b)), causing the edge contact on gear 3. The dislocations of the center contact point in Case C also increases greatly from zero (Figure-4(c)) to 1.97 mm (Figure-8(c)). However, the distributions of contact points and contact ellipses in this case are very small, and can avoid the inducement of edge contact on gear 3. Yet again, the transmission error in Case C $(\Delta\phi_{3'} = 4.9 arc\sec)$ is smaller than those in Cases A $(\Delta\phi_{3'} = 8.2 arc\sec)$ and B $(\Delta\phi_{3'} = 11.8 arc\sec)$, and this can be negligible, as shown in Figure-9.

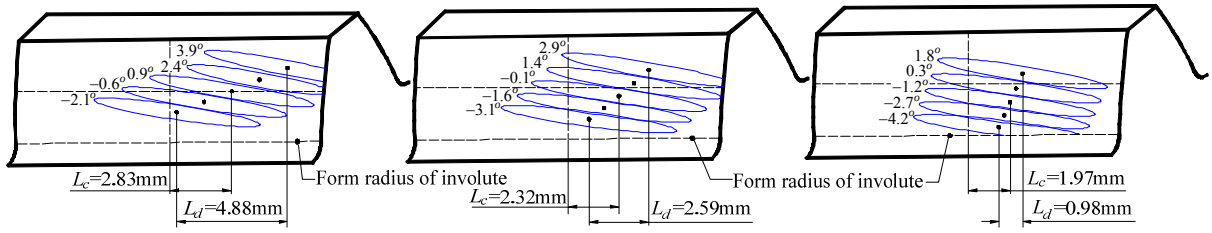

(a)Case A (b)Case B (c)Case C

Figure-8. Simulated tooth contact ellipses and contact points with horizontal misalignment $\Delta\gamma_h = 0.1^\circ$.

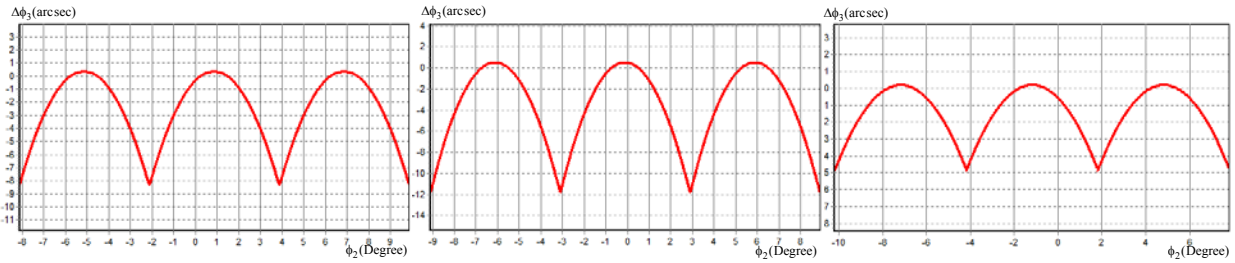

(a)Case A (b)Case B (c)Case C

Figure 9. Transmission errors with horizontal misalignment $\Delta\gamma_h = 0.1^\circ$.

CONCLUSIONS

The effect of the assembly errors on the distribution of contact points in the longitudinal direction is small in the conventional; VTT and proposed methods. These errors do have a notable effect on the dislocation of the center contact point, which is the main cause of edge contact on the double-crowned gear in the conventional and VTT cases. Such center contact point dislocation is particularly affected by the vertical misaligned angle and the horizontal misaligned angle and is not sensitive to the center distance error. The transmission errors of the proposed gear set are in fact a parabolic function, and the maximum magnitude of transmission errors in Case C (our proposed method) is not only smaller than those in Cases A (conventional) and B (VTT) but negligible.

REFERENCES

[1] F.L. Litvin, A. Fuentes. 2004. Gear Geometry and Applied Theory. The second ed., Cambridge University Press.

[2] F.L. Litvin, P.H. Peng, S.A. Lagutin, D.P. Townsend, T.M. Sep. 2001. United States Patent No. US 6205 879 B.

[3] F.L. Litvin, A. Fuentes, I.G. Peres, L. Carvenali, K. Kawasaki, R.F. Handschuh. 2003. Modified Involute Helical Gears: Computerized Design, Simulation of Meshing and Stress Analysis.Computer Methods in Applied Mechanics and Engineering. 192: 3619-3655.

[4] F.L. Litvin, I.G. Peres, A. Fuentes, K. Hayasaka, K. Yukishima. 2005. Topology of Modified Surfaces of Involute Helical Gears with Line Contact Developed for Improvement of Bearing Contact, Reduction of Transmission Errors, and Stress Analysis. Mathematical and Computer Modeling. 42: 1063-1078.

[5] W.S. Wang, Z.H. Fong. 2008. A Dual Face-HobbingMethod for the Cycloidal Crowning of Spur Gear.Mechanism and Machine Theory. 43: 1416-1430.

[6] O. Winkel. 2010. New Developments in Gear Hobbing, Gear Technology: 47-55.

[7] R.H. Hsu, Z.H. Fong. 2011. Novel Variable-Tooth-Thickness Hob for Longitudinal Crowning in the Gear-Hobbing Process. Thirteenth World Congress in

Mechanism and Machine Science, Gearing and Transmissions, Guanajuato, Mexico.

[8] C.B. Tsay. 1988. Helical Gears with Involute Shaped Teeth: Geometry, Computer Simulation, Tooth Contact Analysis, and Stress Analysis. ASME Journal of Mechanical Design. 110: 482-491.

[9] R.H. Hsu, H.H. Su. 2014. Tooth Contact Analysis for Helical Gear Pairs Generated by a Modified Hob with Variable Tooth Thickness. Mechanism and Machine Theory. 71: 40-51.

[10] V.T. Tran, R.H. Hsu and C.B. Tsay. 2014. Study on the Anti-Twist Helical Gear Tooth Flank With Longitudinal Tooth Crowning. ASME Journal of Mechanical Design. p. 136.

[11] V.T. Tran, R.H. Hsu and C.B.Tsay. 2014. A Novel Finish Hobbing Methodology for Longitudinal Crowning of a Helical Gear with Twist-Free Tooth Flanks by Using Dual-Lead Hob Cutters.ASME 2014 International Mechanical Engineering Congress and Exposition, Montreal, Quebec, Canada. Paper No. IMECE2014-36149: 1-9.

[12] V.T. Tran, R.H. Hsu and C.B. Tsay. 2015. Tooth Contact Analysis for a Double-Crowned Involute Helical Gear with Twist-Free Tooth Flanks Generated by Dual-Lead Hob Cutters. ASME Journal of Mechanical Design 137.